JACS
JOURNAL OF THE AMERICAN CHEMICAL SOCIETY
pubs.acs.org/JACS
Article

Liver-Detargeted Aromatic Bioreducible mRNA Lipid Nanoparticles Confer Lymph Node Tropism and Robust Antigen-Specific Immunity

Hannah M. Yamagata, Marshall S. Padilla, Alex G. Hamilton, Kelsey L. Swingle, Ajay S. Thatte, Adele S. Ricciardi, Anushka Agrawal, Emily Fitzgerald, Alexandre J. Poirier, Hannah C. Geisler, Ryann A. Joseph, Ori Z. Chalom, Sherry Du, Jacqueline J. Li, Dongyoon Kim, Ricardo C. Whitaker, Christian G. Figueroa-Espada, Emily L. Han, Amanda M. Murray, Mohamad-Gabriel Alameh, Drew Weissman, and Michael J. Mitchell*

Cite This: J. Am. Chem. Soc. 2026, 148, 14137−14150
Read Online
ACCESS | Metrics & More | Article Recommendations | Supporting Information

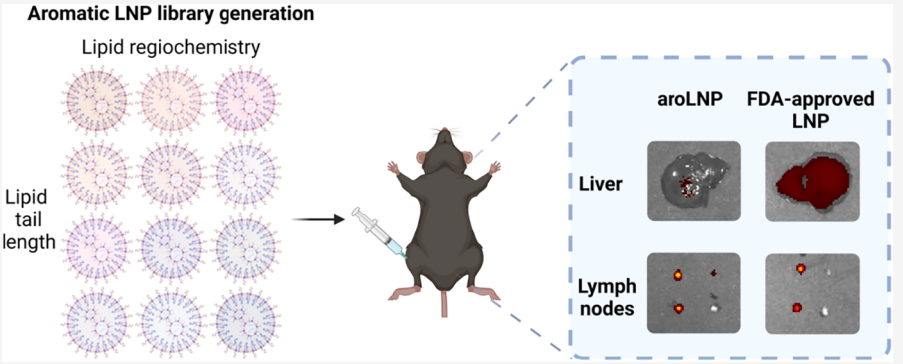

ABSTRACT: Lipid nanoparticles (LNPs) have been immensely successful in facilitating the delivery of nucleic acids to tissues of interest and continue to be optimized for mRNA delivery. These vehicles are particularly advantageous for vaccination due to their ease of production, highly tunable composition, and ability to induce robust immune responses without an adjuvant, as exemplified most recently by the clinical success of the Pfizer/BioNTech and Moderna COVID-19 vaccines. However, LNPs are known to exhibit off-target liver tropism. To address this limitation, we developed a library of aromatic bioreducible ionizable lipids that potently transfect secondary lymphoid tissues with liver detargeting capabilities compared with an industry standard ionizable lipid used in the COVID-19 vaccine. The library consists of three modular components: amine core structure, lipid tail length, and regiochemistry. These aromatic ionizable lipids employ benzene rings both as a scaffold for regiochemical differences and as a moiety to improve transfection. Bioreducible disulfide bonds in the lipids additionally serve to increase their biodegradability. When these aromatic ionizable lipids are formulated as LNPs, top-performing aromatic LNPs (aroLNPs) accumulate in and transfect lymph nodes while minimizing off-target liver tropism. Top-performing aroLNPs also induce strong antigen-specific immune responses, increased effector memory T cell generation, and decreased terminal effector T cell generation in mice when utilized in a preclinical SARS-CoV-2 vaccine study. Additionally, aroLNPs are strongly retained in the injection site and induce low levels of systemic inflammatory cytokines. Together, these results establish aroLNPs as a promising platform for vaccine delivery and potentially other immune-focused therapeutic applications.

1. INTRODUCTION

Lipid nanoparticles (LNPs) are the most clinically advanced class of nonviral vectors for nucleic acid delivery and vaccine applications, as demonstrated by their use in the U.S. Food and Drug Administration (FDA)-approved Pfizer/BioNTech and Moderna COVID-19 mRNA vaccines.[1,2] These carriers are particularly advantageous due to their innate biocompatibility stemming from their PEG lipid coating and lack of immunogenic viral proteins.[3] Their common use of mRNA as cargo further circumvents potential genotoxicity, a concern often associated with viral vectors.[4] LNPs are typically composed of four lipid components: an ionizable lipid, a helper lipid, cholesterol, and a PEGylated lipid. Each lipid plays a different role in the formation and structural properties of the LNP. Namely, the ionizable lipid

Received: January 3, 2026
Revised: February 11, 2026
Accepted: February 13, 2026
Published: March 24, 2026

https://doi.org/10.1021/jacs.6c00080
J. Am. Chem. Soc. 2026, 148, 14137−14150

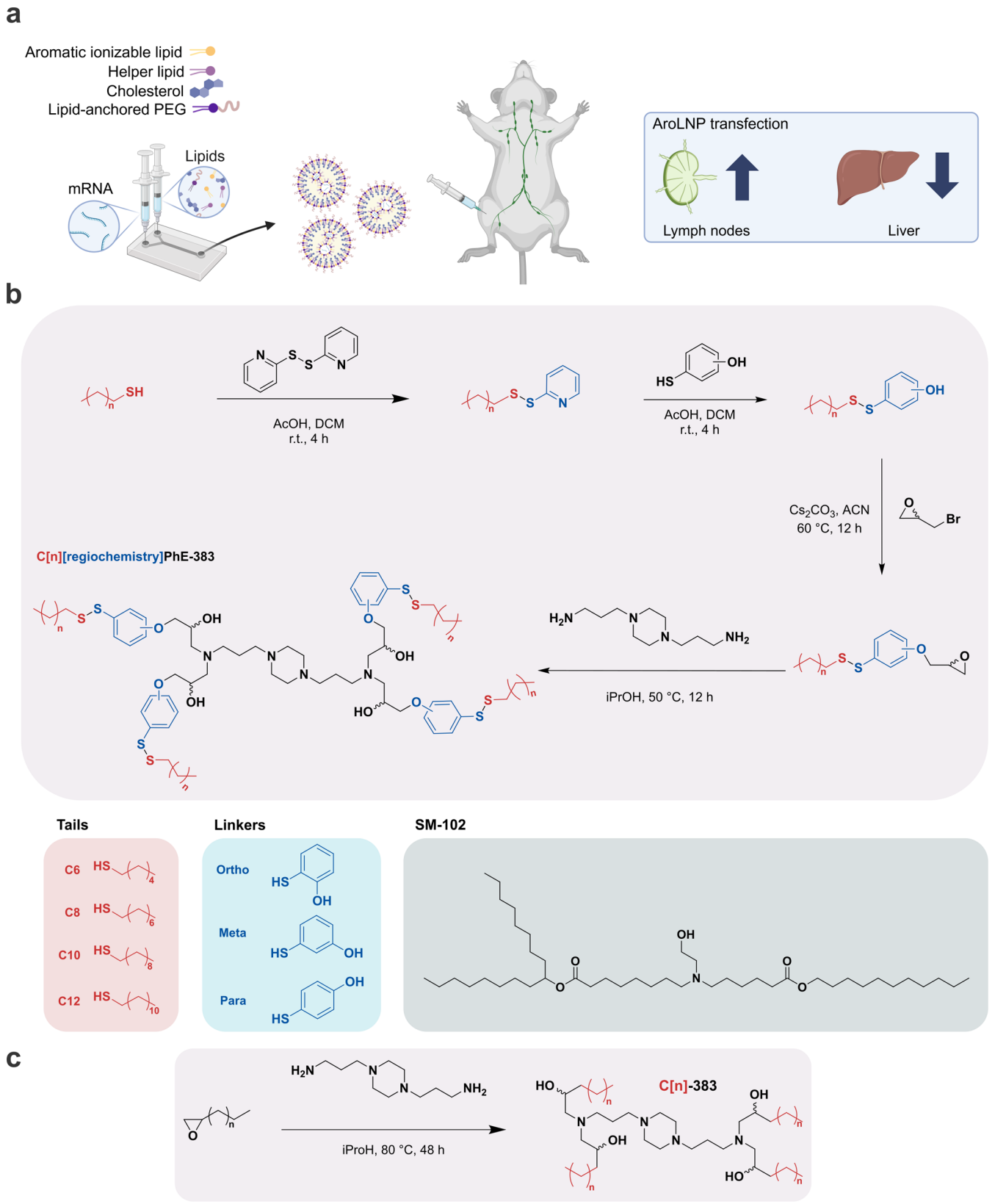

Figure 1. Synthetic scheme of aromatic ionizable lipids with lymph node tropism and reduced hepatic delivery. (a) Illustration of LNP formulation via microfluidic mixing and schematic representation of LNP tropism and transfection following intramuscular (i.m.) administration. (b) Schematic of aromatic ionizable lipid synthesis route, with varying linker regiochemical conformations (blue) and lipid tail lengths (red), and multiple bioreducible disulfide bonds, along with the structure of SM-102, which is used as a benchmark. (c) Synthetic route of control lipids lacking both aromaticity and bioreducible disulfide bonds.

https://doi.org/10.1021/jacs.6c00080
J. Am. Chem. Soc. 2026, 148, 14137−14150

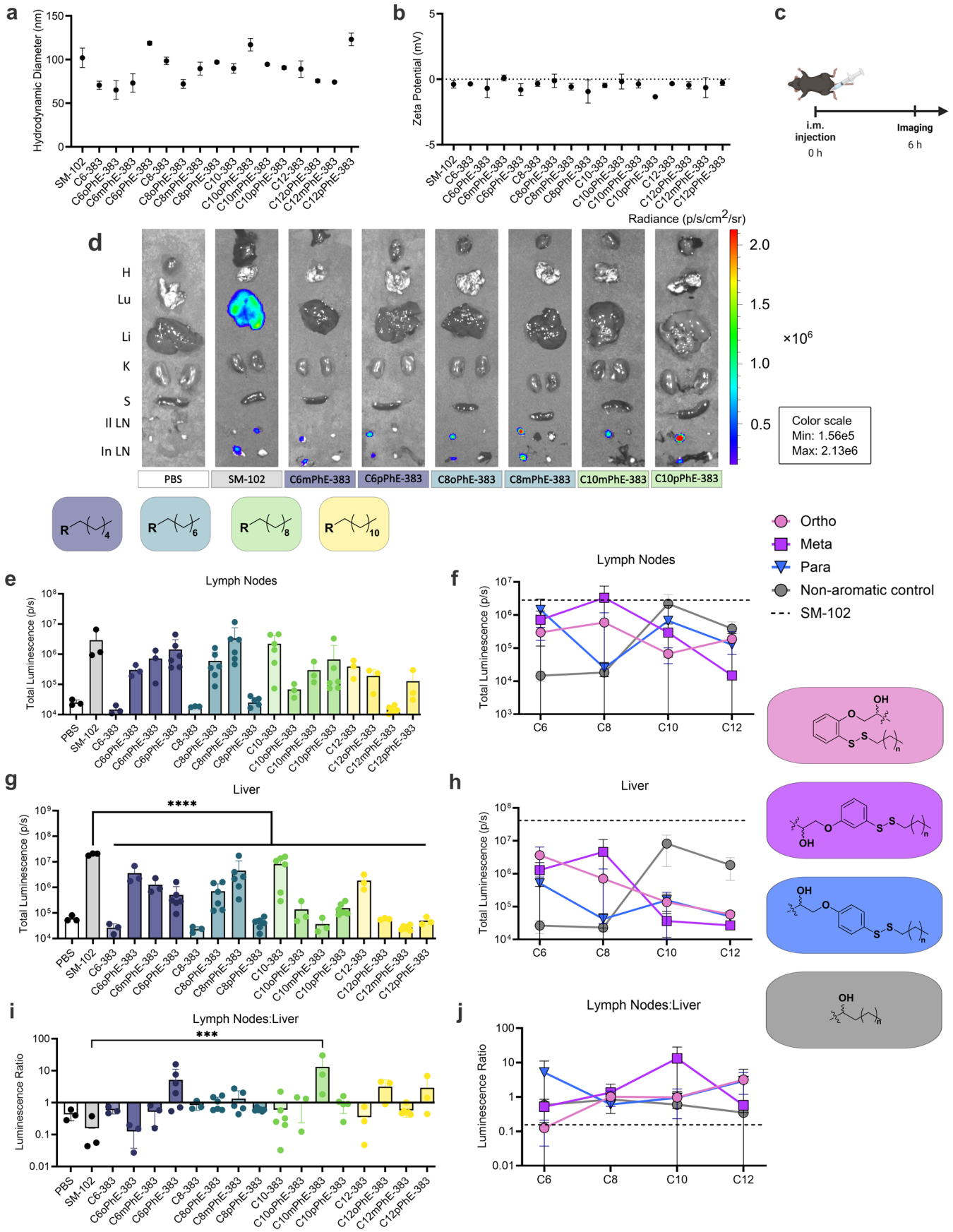

Figure 2. AroLNPs confer strong lymph node transfection with liver detargeting following i.m. administration. (a, b) LNP characterization data for size (a) and ζ-potential (b). (c) Schematic overview of LNP tropism study. (d) *Ex vivo* organ bioluminescence images 6 h after administration of 0.05 mg/kg (1 μg) of luciferase mRNA LNPs. (e–h) Quantification of LNP-mediated transfection in the iliac and inguinal lymph nodes (e, f) and liver (g, h). (i,

https://doi.org/10.1021/jacs.6c00080
J. Am. Chem. Soc. 2026, 148, 14137−14150

Figure 2. continued

j) Relative lymph node to liver luminescence signal. One-way ANOVA with post hoc *t* tests using the Holm−Šídák correction for multiple comparisons was used to compare luminescence and luminescence ratios to SM-102 LNP treatment. H: heart, Lu: lungs, Li: liver, K: kidneys, S: spleen, Il LN: iliac lymph nodes, In LN: inguinal lymph nodes. *$p \leq 0.05$, ****$p \leq 0.0001$.

enables polyanionic mRNA entrapment and endosomal escape, the helper lipid contributes to the structural stability of LNPs, cholesterol modulates LNP membrane integrity, and the PEGylated lipid modifies the surface of the LNP to limit immune recognition and clearance. These components in LNP formulations can be easily tuned, enabling encapsulation of a range of payloads and targeting of specific cells in a variety of diseases.[5] However, LNPs generally exhibit strong hepatic tropism, which could necessitate higher doses and costs per vaccine to achieve potent vaccination.[6] This highlights a strong need to develop a new generation of vaccines that are highly efficacious, yet demonstrate limited liver delivery.

While previous studies have modified LNP formulations to direct mRNA translation and protein expression away from the liver through the addition of a fifth lipid component and active targeting using antibodies or peptides, these strategies require additional steps in LNP manufacturing.[7,8] These approaches are also associated with limitations, including the potential for toxicity from degradation products of these additional lipid components, and complement activation triggered by peptide or antibody conjugation chemistry.[9,10] An attractive alternative strategy to tailor LNP tropism for reduced hepatic accumulation is through structural alterations of the ionizable lipid component of the LNP. The ionizable lipid is a critical component of the LNP formulation due to its key role in RNA encapsulation, endosomal escape, and tropism.[11,12] Indeed, numerous studies have found that small changes to the ionizable lipid structure—whether it be the terminal branching type, number of carbons in the tail, or degree of saturation—can engender significant differences in LNP transfection and tropism.[13−15] One recent study utilized ionizable lipids containing aromatic squaramides to enable potent mRNA delivery to cells.[16] This enhanced performance is thought to be due to $\pi-\pi$ interactions between aromatic moieties and the phosphate backbone of RNA, creating a more stable LNP, as LNPs are typically composed of weaker intermolecular interactions.[16] However, despite this promising mechanistic finding, research into the rational design and application of aromatic ionizable lipids has been limited.

Here, we utilize aromatic rings as scaffolds to develop a library of ionizable lipids for immune organ delivery with limited liver uptake and transfection. By using four rings in each ionizable lipid, we leverage both the benefits of their aromaticity as well as their regiochemical versatility stemming from the easily tunable benzene ring. These lipids are modular in their lipid tail length and regiochemistry and can theoretically be conjugated to nearly any amine core. They also include bioreducible disulfide bonds, which function to increase their biocompatibility. They additionally serve to increase LNP cellular uptake and endosomal escape; as when incorporated into polymeric and lipid nanoparticles, thiols have been shown to substantially increase these metrics.[17−19] The present study represents the first application of such aromatic ionizable lipids in a vaccine context, expanding the design space for immunotropic delivery systems. We demonstrate that top-performing aroLNPs potently deliver mRNA to the lymph nodes and spleen while significantly reducing liver delivery compared to LNPs containing SM-102, an ionizable lipid used in one of the FDA-approved mRNA LNP COVID-19 vaccines. We further evaluated these lipids in a SARS-CoV-2 vaccine study and demonstrated that aroLNPs are able to induce a strong, antigen-specific response against the SARS-CoV-2 spike protein comparable to that of SM-102 LNPs. Additionally, we show that top-performing aroLNPs are strongly retained in the injection site and induce low levels of systemic proinflammatory cytokines. These lipids represent an exciting new platform for immunological LNP applications with limited liver delivery.

2. RESULTS AND DISCUSSION

2.1. Synthesis of Aromatic Ionizable Lipids and LNP Formulation

Amine-based ionizable lipids consist of one or more electrophilic tails conjugated to an amine-containing core. This is a generally facile reaction that can enable the generation of large libraries of lipids. Here, we synthesized a library of lipids with varying tail lengths and regiochemistry to explore how changing each of these moieties affects LNP tropism and mRNA delivery (Figure 1a−b). Bioreducible disulfide bonds were additionally incorporated into each tail of the ionizable lipids to increase their biodegradability. To synthesize each compound, alkanethiols of varying lengths were reacted with 2,2′-dipyridyldisulfide, conjugating the alkanethiol to a pyridine group. The resulting compound was then reacted with a benzene thiol to remove the remaining pyridine group and establish the regiochemistry. An epoxide was then conjugated to the ring, creating a tail structure that was then reacted with polyamine cores via S_N2 reactions. We used the 1,4-bis(3-aminopropyl)piperazine (383) polyamine core for this study due to its ability to preferentially transfect immune cells *in vivo*.[20] Tail lengths of 6, 8, 10, and 12 hydrocarbons were selected to diversify the library while maintaining lengths commonly seen in top-performing ionizable lipids.[21] Lipids were named "C[a]-[b]PhE-383," in which [a] is the number of alkyl carbons in each tail following the disulfide bond, and [b] is the regioisomer identity of the lipid tail; *o*, *m*, and *p* are for lipids with the ortho, meta, and para regiochemistry, respectively.

Lipids lacking disulfide bonds and aromatic rings were also synthesized to assess how the absence of these moieties affects LNP performance (Figure 1c). These lipids were synthesized via S_N2 reactions in which epoxides were reacted with the 383 core to form highly structurally similar yet nonaromatic nor bioreducible lipids. These lipids were named "C[a]-383" in which [a] is the number of alkyl carbons in each tail. LNPs were formulated using a microfluidic device fabricated with staggered herringbone pattern features as previously described.[22] Formulation parameters for aroLNPs and non-aroLNPs were identical, differing only in the structural identity of the ionizable lipid used. As a benchmark, SM-102 was prepared according to its standard lipid composition.[23] Formulated LNPs demonstrated a hydrodynamic diameter between 60 and 120 nm (Figure 2a), a generally neutral ζ-potential (Figure 2b), and an encapsulation efficiency above 80% (Figure S1).

https://doi.org/10.1021/jacs.6c00080
J. Am. Chem. Soc. 2026, 148, 14137−14150

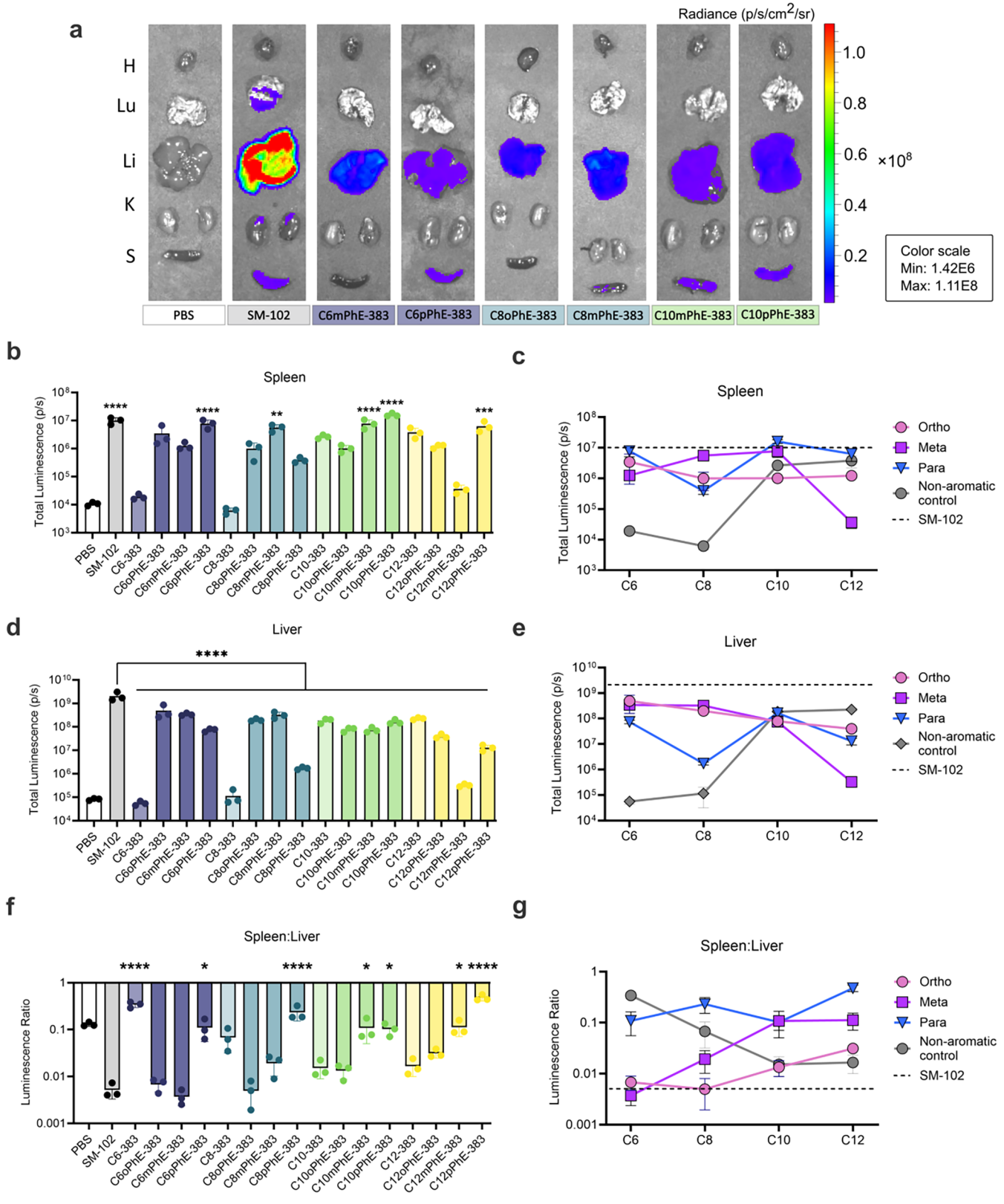

Figure 3. AroLNPs delivered via i.v. administration demonstrate reduced liver tropism. (a–d) LNP transfection in the spleen (a, b) and liver (c, d), after i.v. treatment with LNPs containing luciferase mRNA via tail vein injection. This tropism was also represented as trends between lipids with the same tail lengths yet different regiochemistry for lymph node (c) and liver (e) transfection. (e, f) Relative spleen to liver luminescence signal. (g) *Ex vivo* organ bioluminescence images 6 h after injection. One-way ANOVA with post hoc *t* tests using the Holm–Šídák correction for multiple comparisons were used to compare luminescence and luminescence ratios to PBS (b) and SM-102 LNP treatment (d, f). H: heart, Lu: lungs, Li: liver, K: kidneys, S: spleen. *$p \leq 0.05$, **$p \leq 0.01$, ***$p \leq 0.001$, ****$p \leq 0.0001$.

https://doi.org/10.1021/jacs.6c00080
J. Am. Chem. Soc. 2026, 148, 14137–14150

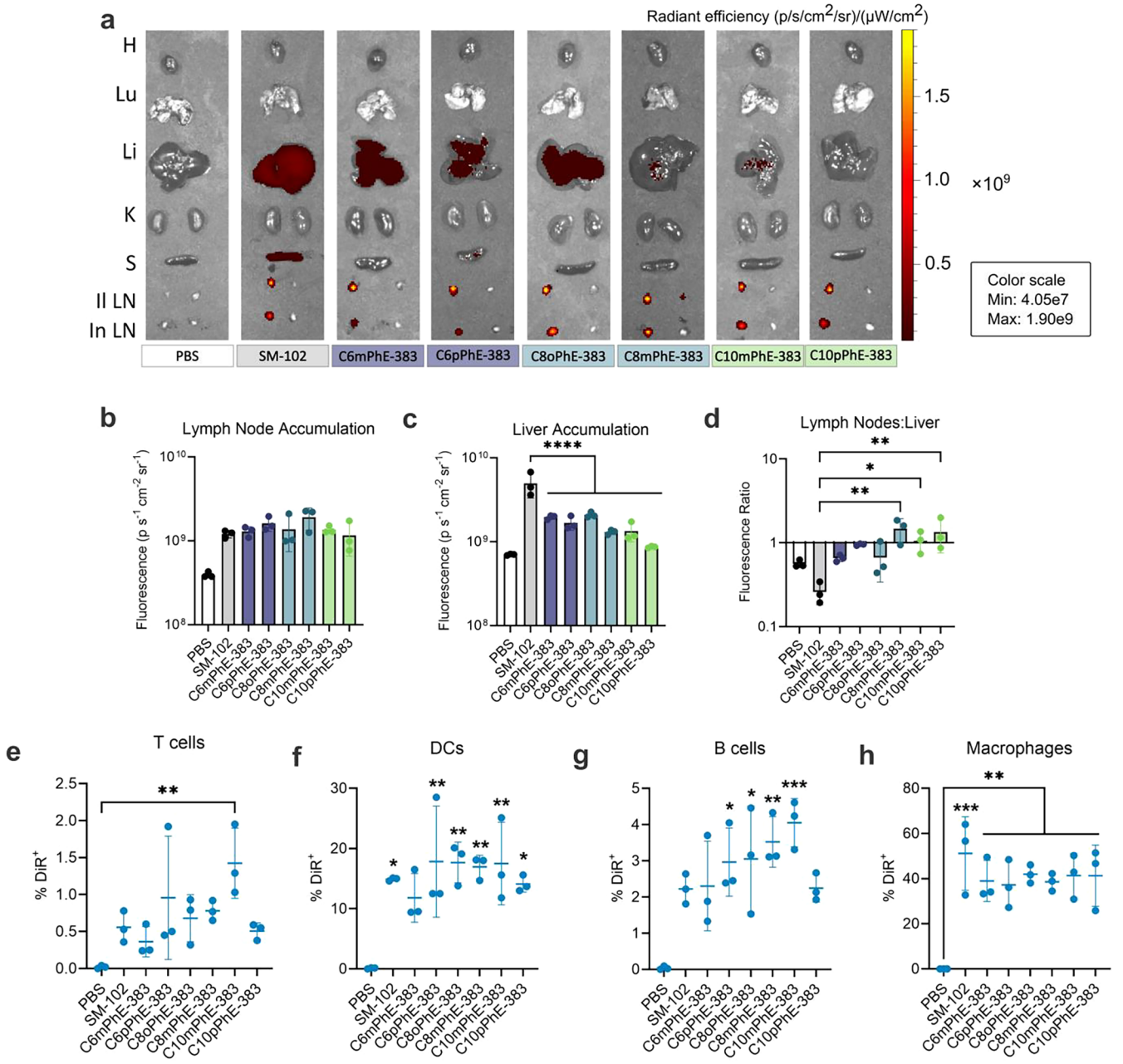

Figure 4. AroLNPs exhibit decreased liver and macrophage accumulation. (a) *Ex vivo* organ fluorescence images 6 h after i.m. injection of top-performing LNPs labeled with DiR. (b, c) Quantification of LNP accumulation in iliac and inguinal lymph nodes (b) and liver (c) 6 h after injection. (d) Relative lymph node-to-liver accumulation as quantified by fluorescence signal. (e–l) Flow cytometric analysis of DiR positivity in $CD3^+$ T cells (e), $CD11c^+$ dendritic cells (DCs) (f), $CD19^+$ B cells (g), and $CD11b^+F4/80^+$ macrophages (h) from iliac and inguinal lymph nodes 6 h post i.m. injection. One-way ANOVA with post hoc Holm–Šídák correction for multiple comparisons was used to compare fluorescence and fluorescence ratios to SM-102 LNP (b–d) and PBS (e–h) treatment groups. H: heart, Lu: lungs, Li: liver, K: kidneys, S: spleen, Il LN: iliac lymph nodes, In LN: inguinal lymph nodes. *$p \leq 0.05$, **$p \leq 0.01$, ***$p \leq 0.001$, ****$p \leq 0.0001$.

2.2. AroLNPs Exhibit mRNA Delivery to Lymph Nodes with Decreased Liver Delivery

Since we expected our 383 polyamine core-based lipids to confer a degree of immune cell tropism, we administered luciferase mRNA aroLNPs intramuscularly (i.m.) to mice at 0.05 mg/kg (1 μg total) to assess tissue-level transfection (Figure 2c). After 6 h, the heart, lungs, liver, kidneys, spleen, and iliac and inguinal lymph nodes were harvested and imaged *ex vivo* (Figure 2d). Mice treated with aroLNPs demonstrated luminescence signal in the lymph nodes comparable to those treated with SM-102 LNPs (Figure 2e,f). Notably, however, mice in all groups demonstrated liver luminescence at least 10-fold lower than that of SM-102 ($p < 0.001$; Figure 2g,h). Shorter length (6 and 8 carbon-tailed) nonaromatic control lipids performed poorly compared to their aromatic counterparts with identical tail lengths in both liver and lymph node transfection (Figure 2f,h), indicating that the aromatic rings and disulfide bonds play a critical role in LNP transfection. Longer length (10 and 12 carbon-tailed) nonaromatic control lipids demonstrated higher levels of lymph node and liver delivery than their aromatic counterparts, possibly indicating that increasingly hydrophobic

https://doi.org/10.1021/jacs.6c00080
J. Am. Chem. Soc. 2026, 148, 14137–14150

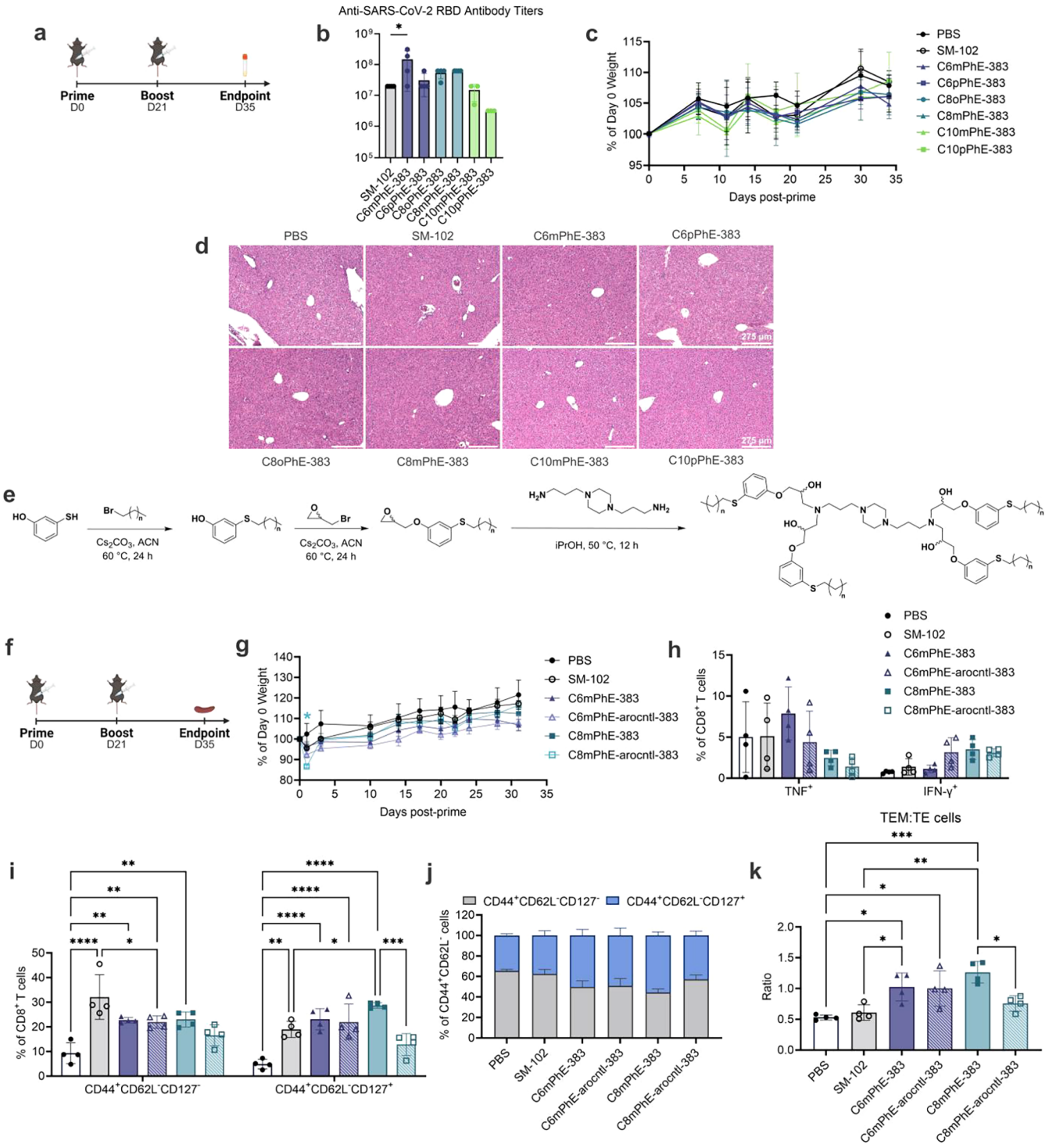

Figure 5. AroLNPs initiate a strong antigen-specific response after administration as a COVID-19 vaccine. (a) Schematic of prime-boost vaccination strategy. Mice were vaccinated with 0.25 mg/kg (5 μg) of SARS-CoV-2 RBD mRNA. (b) Reciprocal endpoint anti-SARS-CoV-2 RBD IgG titers. (c) Mouse weight over time rose steadily for all treatment groups in alignment with the PBS-treated group. (d) H&E stained liver sections from vaccinated mice. (e) Schematic of prime-boost vaccination strategy for the vaccine study in which the spleen was collected at the endpoint. (f) Schematic for aromatic control lipids lacking disulfide bonds. (g) Mouse weight over time after the priming vaccination. (h–k) T cell markers after splenic restimulation with SARS-CoV-2 peptide at the study endpoint. Intracellular TNF and IFN-γ (h) levels were assessed, as was the presence of splenic short-lived terminal effector T cells (T_E cells: $CD44^+CD62L^-CD127^-CD8^+$) and long-lasting effector memory T cell (T_{EM} cells: $CD44^+CD62L^-CD127^+CD8^+$) populations (i, j) and their ratio (k). One-way ANOVAs with post hoc *t* tests using the Holm–Šídák correction for multiple comparisons were used to compare reciprocal endpoint titers and body weights to SM-102 (b) and PBS (c, g). One-way ANOVAs with post hoc *t* tests using the Holm–Šídák correction for multiple comparisons were used to compare T cell populations and T_{EM}/T_E ratios to both SM-102 and PBS, as well as compare aroLNPs to their nonbioreducible counterparts (h–j). *$p \leq 0.05$, **$p \leq 0.01$, ***$p \leq 0.001$, ****$p \leq 0.0001$.

https://doi.org/10.1021/jacs.6c00080
J. Am. Chem. Soc. 2026, 148, 14137−14150

aromatic lipids may not enable as potent mRNA delivery as less hydrophobic, shorter tail-length lipids.

To evaluate the degree of off-target liver transfection, we quantified the lymph node-to-liver luminescence ratio. Most aroLNPs achieved a ratio 5−10× higher than that of SM-102 LNPs, indicating that many of our aroLNPs can strongly transfect the lymph nodes while avoiding hepatic transfection (Figure 2i,j).

2.3. AroLNPs Exhibit Significantly Decreased Liver Transfection Following Intravenous Administration.

After observing strong mRNA delivery to the lymph nodes and reduced mRNA delivery to the liver with aroLNPs, we sought to determine if this trend held for intravenous (i.v.) administration, particularly given that LNPs typically demonstrate strong liver tropism using this delivery route.[24] LNPs encapsulating luciferase mRNA were administered i.v. to mice, following which tissues were harvested after 6 h (Figure 3a). Many aroLNPs demonstrated strong spleen transfection (Figure 3b,c) with mean luminescence values of approximately 10^7 p/s. Additionally, all LNPs assessed exhibited at least 4 times lower mRNA delivery to the liver than SM-102 LNPs (Figure 3c,d). When the spleen-to-liver luminescence ratio was calculated for each of the LNPs, many exhibited a higher ratio than SM-102 LNPs, including C6pPhE-383, C8mPhE-383, C10mPhE-383, and C10pPhE-383 aroLNPs (Figure 3e,f). These LNPs similarly exhibited a lymph node-to-liver mRNA delivery ratio higher than that of SM-102 when delivered i.m., as well as high levels of both spleen and lymph node delivery, supporting the conclusion that these lipids are immunotropic. Overall, these results suggest that our aromatic ionizable lipids substantially decrease liver transfection following both i.m. and i.v. administration. Interestingly, the synergistic influence of regiochemistry and tail length on transfection efficacy appears to be conserved across the two administration routes tested (Figure 3c,e,3g). This result suggests that regiochemistry differences play a substantial role in transfection trends between lipids in a manner agnostic of the delivery route.

2.4. AroLNPs Accumulate Primarily in the Lymph Nodes after Intramuscular Administration

Having determined that aroLNPs primarily transfected the lymph nodes following i.m. administration, we sought to determine if they also accumulated mainly in these tissues. Since LNP toxicity can occur from the accumulation of LNPs that do not successfully undergo endosomal escape or enter the cell, LNPs demonstrating not only low transfection in nonimmune tissues but also reduced accumulation in these tissues could help to decrease overall off-target toxicity.[25] We selected immunotropic aroLNPs with relatively strong lymph node and spleen delivery when administered i.m. and i.v., respectively, and a high lymph node-to-liver transfection ratio. LNPs were formulated with luciferase mRNA, dyed with lipophilic DiR, and delivered i.m. to mice. When organs were imaged *ex vivo* (Figure 4a), we found that the accumulation profiles aligned well with transfection results. Indeed, all aroLNPs accumulated in the lymph nodes at a level similar to or greater than that of SM-102 LNPs (Figure 4b). Strikingly, all aroLNPs exhibited at least 2.7× lower liver accumulation than SM-102 (Figure 4c). Thus, when the lymph node-to-liver accumulation ratio was calculated for all LNPs tested, all aromatic formulations outperformed SM-102 (Figure 4d), suggesting that aroLNPs mainly traffic to the lymph nodes when delivered i.m.

Having observed promising tissue-level accumulation results, we next investigated which cell types within the lymph nodes aroLNPs were targeting using flow cytometry (Table S1 and Figure S2). We found that most aroLNPs accumulated in T cells at levels similar to those of SM-102 LNPs, with the exception of C10mPhE-383 aroLNPs, which accumulated 2.5× more in T cells than the control (Figure 4e). Furthermore, C6mPhE-383 and C10pPhE-383 aroLNPs demonstrated ∼3% lower and approximately equal accumulation in dendritic cells (DCs), respectively, while all other aroLNPs exhibited ∼3% higher levels of accumulation (Figure 4f). These results aligned well with DiR mean fluorescence intensity (MFI) in the cell populations of interest (Figure S3). DCs are especially attractive targets for vaccines, as vaccines require exposure of antigens to antigen-presenting cells (APCs).[26] DCs are particularly beneficial APCs to deliver to due to their key role in initiating potent $CD8^+$ T cell activation.[27,28] Notably, C6pPhE-383, C8oPhE-383, C8mPhE-383, and C10mPhE-383 aroLNPs all exhibited comparatively increased accumulation in DCs, which may make them promising candidates for vaccines.

AroLNPs tended to accumulate in B cells at an approximately equal or higher percentage than SM-102 LNPs (Figure 4g). This result further highlights the potential of aroLNPs as strong candidates for vaccines due to the role of B cells as professional APCs.[29] All aroLNPs tested demonstrated uptake in macrophages ∼10% lower than that of the control, with ∼ 40% DiR positivity for all formulations (Figure 4h). Since liver uptake has been found to correspond with macrophage uptake, particularly uptake in Kupffer cells, this lower level of uptake may be a contributing factor to reduced liver delivery by aroLNPs.[30]

2.5. AroLNPs Induce Strong Antigen-Specific Titers after SARS-CoV-2 Vaccination

Since top-performing aroLNPs demonstrated a strong tropism for secondary lymphoid tissue, we sought to evaluate their performance as vehicles for vaccination. We conducted a SARS-CoV-2 vaccine study at a 3-week prime-boost interval, followed by an endpoint 2 weeks after the booster dose (Figure 5a). Mice were vaccinated with top-performing aroLNPs or SM-102 control LNPs encapsulating SARS-CoV-2 S2P mRNA. Two weeks after the boost dose, mouse sera were collected for analysis of endpoint anti-SARS-CoV-2 receptor binding domain (RBD) antibody titers. All LNPs assessed aside from the C10pPhE-383 formulation exhibited high reciprocal endpoint antigen-specific IgG titers with values ranging from approximately $10^{7.3}$ to $10^{8.3}$ (Figure 5b). For lipids of the same length, these data suggest that lipids in the meta conformation are potentially more immunogenic and stronger vaccine candidates than their para counterparts, although this is a point of investigation for future work.[31] Mouse weight was measured over time and was found to increase steadily in all treatment groups, comparably to PBS, indicating a lack of acute toxicity from any of the LNPs (Figure 5c). To further investigate potential LNP toxicity, mouse livers were collected, stained for hematoxylin and eosin (H&E), and imaged (Figure 5d). All mouse liver sections lacked inflammatory cell infiltration and tissue damage characteristic of acute toxicity, further supporting that aroLNPs are not acutely toxic.[32]

2.6. Disulfide Bonds Aid in Increasing aroLNP Transfection Efficiency

We next sought to explore how aroLNP adjuvanticity, delivery, and toxicity are affected by the absence of disulfide bonds. When incorporated into ionizable lipids used in LNPs, disulfide bonds

https://doi.org/10.1021/jacs.6c00080
J. Am. Chem. Soc. 2026, 148, 14137−14150

have been shown to increase cellular uptake, endosomal escape, and cytoplasmic location of mRNA.[33,34] Although the exact mechanism is unknown, it is hypothesized that this arises from covalent interactions, namely disulfide exchange reactions, between thiols on the cellular membrane and within LNPs straining endosomal membrane packing and resulting in endosomal rupture and escape.[17,35] Further, disulfide bonds are easily reduced in the cellular environment due to their high responsiveness to glutathione.[17] As such, they are of particular interest and hypothesized to aid aroLNPs in both their biocompatibility and delivery.

To assess this hypothesis, we synthesized aromatic ionizable lipids identical to our top-performing vaccine lipid (C6mPhE-383) and our top-performing lymph node transfection lipid (C8mPhE-383) without disulfide bonds (Figure 5e). This involved first reacting a bromoalkane with a benzene thiol to create an aromatic tail with a tail length of interest, followed by conjugation of an epoxide to the benzene ring to form a final aromatic nonbioreducible tail structure. This tail was then reacted with 383 core via an S_N2 reaction to synthesize the final ionizable lipid. These control lipids were named C[a]-[b]PhE-arocntl-383 in which [a] is the number of alkyl carbons in each tail, and [b] is the regiochemistry of the lipid as established in the naming of the original aroLNP library. When formulated as LNPs, these control LNPs were monodisperse and had larger hydrodynamic diameters around 145−180 nm, high encapsulation efficiencies >80%, and a slightly negative ζ-potential around −6 mV (Figure S4a−c).

To assess the biodistribution of these lipids, we formulated LNPs with luciferase mRNA and administered LNPs i.m. to mice. We found that the aromatic control lipids had similar, albeit slightly decreased (<3-fold), transfection in the lymph nodes when compared to their bioreducible counterparts. C6mPhE-arocntl-383 and C8mPhE-arocntl-383 LNPs also had ∼30-fold and ∼60-fold increased lymph node transfection when compared to their nonaromatic nor bioreducible counterparts, respectively (Figure S4d). The aromatic control LNPs also demonstrated significantly reduced liver delivery compared with SM-102 LNPs. Notably, their liver transfection was greater than that of their nonaromatic nor bioreducible counterparts but less than that of their aroLNP counterparts, suggesting that the benzene rings and disulfide bonds play synergistic roles in LNP transfection efficiency (Figure S4e,f).

To better understand how disulfide bonds affect cell-specific transfection, as well as compare lymphatic cell-specific accumulation and transfection for our top-performing vaccine aroLNP, we further assessed C6mPhE-arocntl-383 LNPs and C6mPhE-383 aroLNPs using a Cre-lox system with Ai9 mice (Table S2 and Figure S5). Ai9 mice have a *loxP*-flanked STOP cassette in their genome, which causes them to express tdTomato following Cre-mediated excision of these cassettes, enabling quantification of cell-specific transfection in the lymph nodes. Since the magnitude of LNP accumulation when measuring dyed LNPs tends to be greater than the magnitude of LNP transfection calculated with protein reporter fluorophores, the percentage of cells transfected across all immune cells is lower for all LNPs, but the trends between SM-102 LNPs and C6mPhE-383 aroLNPs remained highly similar to earlier accumulation data after i.m. administration (Figures 4e−h and S6a−d). C6mPhE-arocntl-383 LNPs exhibited similar transfection in T cells to their aroLNP counterpart, transfecting a significantly lower proportion of T cells than SM-102 (Figure S6a). However, since vaccination relies upon APC presentation to T cells rather than delivery to T cells themselves, of more importance is APC transfection.[26] C6mPhE-arocntl-383 LNP transfection resulted in a similar proportion of tdTomato$^+$ DCs, B cells, myeloid cells, and macrophages to SM-102, suggesting that the aromatic control may be a strong vaccine LNP (Figure S6b−e).

2.7. Effector Memory T Cell Generation Is Increased after aroLNP Vaccination

To further assess the immunogenic capabilities of top aroLNPs C6mPhE-383 and C8mPhE-383 and better understand the role of bioreducibility in their performance, we formulated these LNPs and their aromatic control counterparts with SARS-CoV-2 S2P mRNA and vaccinated mice as described above (Figure 5f). Notably, 24 h after the priming dose, mice receiving the C6mPhE-arocntl-383 and C8mPhE-arocntl-383 vaccines lost approximately 8% (p = 0.092) and 13.5% (p = 0.039) of their initial body weight, respectively (Figure 5g). These groups recovered weight by Day 3, suggesting acute toxicity. Mice treated with aroLNPs did not experience a similar weight loss, suggesting that disulfide bonds aid in improving lipid biocompatibility and reducing LNP-mediated toxicity.

Two weeks after the booster dose, mouse spleens were collected and restimulated with SARS-CoV-2 peptide to assess the cell-mediated immunity conferred by each LNP (Table S3 and Figure S7). We found that C6mPhE-383 aroLNP-treated mice exhibited elevated levels of tumor necrosis factor (TNF) in CD8$^+$ T cells relative to those of other assessed LNPs. Further, aromatic control LNP- and C8mPhE-383 aroLNP-treated mice exhibited increased interferon-γ (IFN-γ) levels in CD8$^+$ T cells (Figure 5h). The proportions of TNF$^+$ and IFN-γ^+ CD4$^+$ T cells stimulated by LNPs followed similar trends, although IFN-γ^+ for all groups was notably decreased (Figure S8a,b). We additionally assessed the abundance of terminal effector (T_E) and effector memory T (T_{EM}) cells, as T_{EM} cell generation is critical to achieving long-lasting immunity from a vaccine, while T_E cells are short-lived and have limited recall potential, thereby making them less favorable.[36−38] We define T_{EM} cells as CD44$^+$CD62L$^-$CD127$^+$CD8$^+$ T cells and T_E cells as CD44$^+$CD62L$^-$CD127$^-$CD8$^+$ T cells. Mice treated with aroLNPs had decreased T_E cells and increased T_{EM} cells compared to SM-102-treated mice, with C8mPhE-383-treated groups having a significantly higher T_{EM} population (Figure 5i,j). When the ratio of T_{EM}/T_E populations was calculated for each group, aroLNP-treated mice again demonstrated a significantly higher preference for T_{EM} cell generation, further supporting their potential as a strong platform for potent vaccination (Figure 5k).

Interestingly, the C8mPhE-383-treated group generated significantly more T_{EM} cells and had a significantly higher T_{EM}/T_E ratio than the C8mPhE-arocntl-383-treated group, indicating that a lack of bioreducibility in the aromatic lipids may hinder their ability to mount an effective immune response. However, C6mPhE-arocntl-383-treated mice generated highly similar proportions of T_{EM} cells and T_E cells to the C6mPhE-383-treated group, suggesting that the structure−function relationship between aroLNPs and their aromatic control counterparts may be more involved, despite these lipids being only two carbons in tail length different.

2.8. AroLNPs Demonstrate Increased Retention in the Injection Site and ApoE Independence

Having identified two aroLNPs that are able to both highly transfect immune reservoirs and demonstrate therapeutic

https://doi.org/10.1021/jacs.6c00080
J. Am. Chem. Soc. 2026, 148, 14137−14150

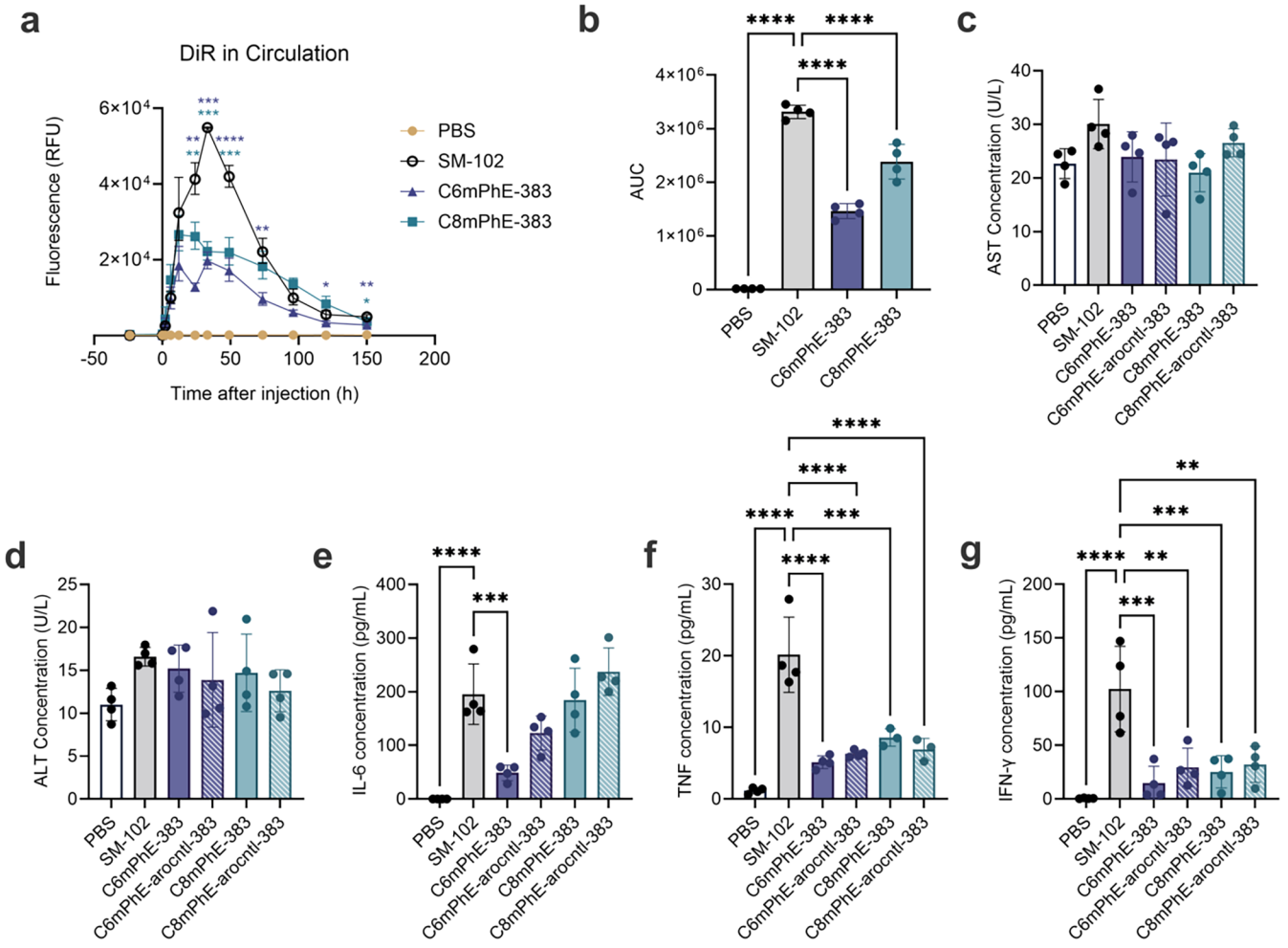

Figure 6. AroLNPs are retained in the injection site and disulfide bonds aid in reducing systemic IL-6 production. (a) LNP systemic circulation over time after DiR-dyed LNP injection. (b) AUC of LNP leakage into circulation over time. (c–g) Mice were i.m. administered luciferase mRNA LNPs, and serum was collected and assessed for AST (c) and ALT (d) via a colorimetric assay. Serum was also analyzed for IL-6 (e), TNF (f), and IFN-γ (g) concentration via ELISA. One-way ANOVAs with post hoc t tests using the Holm–Šidák correction for multiple comparisons were used to compare LNP leakage into circulation and the calculated resulting AUC, as well as all proinflammatory cytokine concentrations to SM-102 LNPs (a–g). *$p \leq 0.05$, **$p \leq 0.01$, ***$p \leq 0.001$, ****$p \leq 0.0001$.

efficacy in a vaccine model, we next sought to investigate how aroLNPs can detarget the liver and achieve strong lymph node tropism. We hypothesized that aroLNPs may be more highly retained in the injection site, causing decreased systemic circulation and less opportunity for aroLNPs to interface with the liver. Since LNPs retained in the muscle tend to preferentially drain into the lymphatic system, this retention could also be driving their lymphoid organ tropism.[39,40] To assess this, we dyed aroLNPs encapsulating luciferase mRNA with DiR, injected them i.m. into mice, and collected blood at regular intervals. We then estimated the amount of LNP present through fluorescence imaging on mouse sera. Through this assay, we found that aroLNPs leaked into circulation significantly less than SM-102 LNPs, with fluorescence peaking in mouse sera around 12 h after injection, while SM-102 LNPs continued to leak into circulation until reaching a fluorescence peak around 36 h (Figure 6a). The area under the curve (AUC) of each trace in Figure 6a was calculated, and the aroLNPs had significantly lower AUCs than SM-102, indicating that they are well-retained in the injection site, potentially playing a role in their ability to achieve liver detargeting and drain into the lymphatic system.[41]

We next assessed aroLNP biodistribution in apolipoprotein E knockout mice ($ApoE^{-/-}$) to probe how aroLNP biodistribution is affected by ApoE for the portion of LNPs that can leak into the bloodstream. ApoE typically plays a key role in LNP protein corona formation and drives LNP uptake to liver hepatocytes.[30] As such, it is possible to shift LNP tropism away from the liver through changing how LNPs interact with serum proteins.[42] After injecting $ApoE^{-/-}$ mice i.m. with aroLNPs carrying luciferase mRNA, we found that liver transfection decreased for SM-102 LNPs approximately 10-fold while lymph node transfection remained similar (Figure S9a,b). We also assessed C12-200, an academic standard LNP with an excipient lipid makeup identical to that of aroLNPs, and found similar results. Despite this, we found that aroLNP liver and lymph node delivery instead increased in $ApoE^{-/-}$ mice, suggesting that aroLNPs interact with ApoE differently than other high-performing LNPs, which may play a role in their liver detargeting abilities. Given the immunological complexity of $ApoE^{-/-}$ mice, aroLNP serum protein interactions remain a point of investigation for future studies.

https://doi.org/10.1021/jacs.6c00080
J. Am. Chem. Soc. 2026, 148, 14137–14150

2.9. Disulfide Bonds Mitigate Toxicity

To determine if systemic toxicity is mitigated by disulfide bonds in aroLNPs, we formulated LNPs with luciferase mRNA and administered to mice i.m., followed by serum collection for analysis via ELISA. In line with prior histology results, we found that aroLNPs do not induce AST and ALT levels significantly higher than those in PBS (Figure 6c,d). These levels are similar to those of SM-102-treated mice, indicating a lack of liver toxicity by all LNPs assessed. However, the levels of systemic interleukin-6 (IL-6), TNF, and IFN-γ were all highly significantly increased in groups treated with SM-102 (Figure 6e−g). Strikingly, all assessed aroLNPs and nonbiodegradable aromatic LNPs caused a significant, strong reduction in systemic TNF and IFN-γ secretion. Since these LNPs all demonstrate significantly decreased liver transfection compared to SM-102, these results highlight the importance of liver detargeting in reducing systemic TNF and IFN-γ production. This reduction in systemic inflammatory cytokine production is consistent across TNF, IFN-γ, and IL-6 for aroLNP C6mPhE-383, highlighting its strong and significantly increased biocompatibility compared to SM-102 LNPs. Although it is highly desirable to have increased TNF and IFN-γ in splenic T cells after vaccination, as these cytokines aid in immune activation and effector vaccine-induced cellular immunity, they can have detrimental effects when produced systemically.[31] This includes widespread inflammation, cytokine release syndrome, cardiac toxicity, and autoimmunity.[43−47] As these LNPs delivered reporter mRNA, these results point to toxicity induced by the LNPs themselves rather than spike protein production.

The IL-6 serum concentration of mice treated with C6mPhE-383 aroLNPs was significantly below that of groups treated with SM-102 LNPs, highlighting the potential of C6mPhE-383 as a potent and biocompatible vaccine lipid. Notably, nonbioreducible aromatic control LNPs caused elevated levels of IL-6 secretion compared to their bioreducible counterparts. This observation suggests that the disulfide bonds aid in reducing LNP-mediated toxicity, specifically through the reduction of IL-6 secretion, as IL-6 is proinflammatory and associated with immunotherapy toxicity.[48−50] This effect was less pronounced in TNF and IFN-γ results, although the trend held for both aroLNPs in the IFN-γ concentration and C6mPhE-383 aroLNPs in the TNF concentration. Overall, these results highlight aroLNP C6mPhE-383 as a promising LNP that not only detargets the liver and confers stronger antigen-specific titers in vaccinated mice, compared with an industry standard LNP, but also mitigates systemic inflammation and toxicity.

3. CONCLUSIONS

LNPs are the most clinically advanced mRNA vaccine delivery vehicles and can potentially transform the way vaccines are developed broadly. LNPs can encapsulate mRNA constructs with a variety of modifications to reduce their innate toxicity and increase their stability and translational efficacy, creating an extremely large design space for vaccines based solely upon mRNA modification.[51] In combination with our ability to modify the four-component LNP makeup and the chemical makeup of these components, this design space expands even more, allowing us to easily modify current LNP vaccines to optimize their performance.[52,53] Due to the liver-tropic nature of LNPs, it is necessary to iterate upon current formulations to build the next generation of highly specific, efficacious vaccines.[54,55]

In this study, we developed a platform composed of highly modular ionizable lipids and demonstrated that top-performing aroLNPs exhibit strong immune organ tropism. Specifically, we found that aroLNPs with tail lengths of six and eight carbons tended to have greater mRNA delivery to organs of interest than their nonaromatic counterparts, while aroLNPs with tail lengths of ten and twelve carbons demonstrated the opposite tendency. This difference could indicate that the performance of aromatic lipids is dependent on lipid hydrophobicity. We further found that aroLNPs exhibit low levels of liver accumulation and strong lymph node accumulation, aligning with the transfection results.

Following i.m. administration, we found that top-performing aroLNPs minimally leak into systemic circulation, providing a potential mechanistic basis for their immune tropism through lymphatic drainage. As a preliminary therapeutic application of this platform, we conducted a SARS-CoV-2 vaccine study using a prime-boost regimen and found that top-performing aroLNPs elicited a robust antigen-specific response, as characterized by strong SARS-CoV-2 serum titers and splenic T_{EM} cell generation alongside reduced short-lived T_E cell generation. Following these promising results highlighting aroLNPs as potent immunotropic vaccine vectors, we next sought to assess their safety profile. Assessment of serum from mice injected i.m. with firefly luciferase reporter mRNA aroLNPs showed that aroLNPs significantly reduced systemic TNF and IFN-γ inflammatory cytokine generation, underscoring their improved biocompatibility above an industry standard LNP. Since disulfide bonds have been found to play a key role in both biodegradability and nanoparticle endosomal escape, we next investigated the relationship between disulfide bonds in aromatic LNPs and resultant toxicity and efficacy. To do this, we synthesized aromatic ionizable lipids identical to top-performing aroLNPs yet lacking disulfide bonds. These aromatic control LNPs exhibited organ transfection stronger than that of nonaromatic, nonbioreducible control LNPs but weaker than that of aroLNPs, indicating that disulfide bonds and aromatic benzene rings may synergistically aid in increasing LNP transfection. Aromatic nonbioreducible control LNPs also caused significant weight loss in mice after vaccination and elevated levels of systemic IL-6 compared to their aroLNP counterparts, indicating that disulfide bonds are important moieties in lipid design to reduce LNP-mediated toxicity.

From this work, we identified a top-performing aroLNP, C6mPhE-383, that demonstrated preferential transfection and accumulation in the lymph nodes, conferred a potent immune response in mice after vaccination, was well-retained in the injection site, and caused minimal systemic cytokine generation after administration *in vivo*. This study represents an exciting exploration of the incorporation of aromatic rings and bioreducible disulfide bonds into ionizable lipids, and we envision the extension of this platform into existing ionizable lipids with amine cores or the incorporation of the aromatic, bioreducible tails onto a variety of other amine cores to engineer LNPs with enhanced safety and efficacy for vaccination and other immune applications.

■ ASSOCIATED CONTENT

Supporting Information

The Supporting Information is available free of charge at https://pubs.acs.org/doi/10.1021/jacs.6c00080.

Materials and methods; LNP encapsulation efficiency; fluorophores used and flow cytometry gating scheme;

https://doi.org/10.1021/jacs.6c00080
J. Am. Chem. Soc. 2026, 148, 14137−14150

biodistribution of nonbioreducible aromatic LNPs; biodistribution of aroLNPs in ApoE$^{-/-}$ mice; characterization data for all lipids synthesized (PDF)

AUTHOR INFORMATION

Corresponding Author

Michael J. Mitchell − *Department of Bioengineering, University of Pennsylvania, Philadelphia, Pennsylvania 19104, United States; Penn Institute for RNA Innovation, Abramson Cancer Center, Institute for Immunology, Cardiovascular Institute, and Institute for Regenerative Medicine, Perelman School of Medicine, Philadelphia, Pennsylvania 19104, United States;* orcid.org/0000-0002-3628-2244; Email: mjmitch@seas.upenn.edu

Authors

Hannah M. Yamagata − *Department of Bioengineering, University of Pennsylvania, Philadelphia, Pennsylvania 19104, United States;* orcid.org/0000-0002-9525-7102

Marshall S. Padilla − *Department of Bioengineering, University of Pennsylvania, Philadelphia, Pennsylvania 19104, United States;* orcid.org/0000-0003-3607-790X

Alex G. Hamilton − *Department of Bioengineering, University of Pennsylvania, Philadelphia, Pennsylvania 19104, United States*

Kelsey L. Swingle − *Department of Bioengineering, University of Pennsylvania, Philadelphia, Pennsylvania 19104, United States;* orcid.org/0000-0001-8475-9206

Ajay S. Thatte − *Department of Bioengineering, University of Pennsylvania, Philadelphia, Pennsylvania 19104, United States;* orcid.org/0000-0001-7372-8893

Adele S. Ricciardi − *Department of Bioengineering, University of Pennsylvania, Philadelphia, Pennsylvania 19104, United States*

Anushka Agrawal − *Department of Bioengineering, University of Pennsylvania, Philadelphia, Pennsylvania 19104, United States*

Emily Fitzgerald − *Department of Bioengineering, University of Pennsylvania, Philadelphia, Pennsylvania 19104, United States*

Alexandre J. Poirier − *Department of Bioengineering, University of Pennsylvania, Philadelphia, Pennsylvania 19104, United States*

Hannah C. Geisler − *Department of Bioengineering, University of Pennsylvania, Philadelphia, Pennsylvania 19104, United States;* orcid.org/0000-0001-6455-8183

Ryann A. Joseph − *Department of Bioengineering, University of Pennsylvania, Philadelphia, Pennsylvania 19104, United States;* orcid.org/0000-0002-0795-6094

Ori Z. Chalom − *Department of Bioengineering, University of Pennsylvania, Philadelphia, Pennsylvania 19104, United States*

Sherry Du − *Department of Bioengineering, University of Pennsylvania, Philadelphia, Pennsylvania 19104, United States;* orcid.org/0009-0008-8093-1919

Jacqueline J. Li − *Department of Bioengineering, University of Pennsylvania, Philadelphia, Pennsylvania 19104, United States;* orcid.org/0000-0002-7849-5483

Dongyoon Kim − *Department of Bioengineering, University of Pennsylvania, Philadelphia, Pennsylvania 19104, United States;* orcid.org/0000-0002-1769-6505

Ricardo C. Whitaker − *Department of Bioengineering, University of Pennsylvania, Philadelphia, Pennsylvania 19104, United States*

Christian G. Figueroa-Espada − *Department of Bioengineering, University of Pennsylvania, Philadelphia, Pennsylvania 19104, United States;* orcid.org/0000-0003-2700-7678

Emily L. Han − *Department of Bioengineering, University of Pennsylvania, Philadelphia, Pennsylvania 19104, United States;* orcid.org/0009-0008-6276-7502

Amanda M. Murray − *Department of Bioengineering, University of Pennsylvania, Philadelphia, Pennsylvania 19104, United States;* orcid.org/0009-0000-2124-351X

Mohamad-Gabriel Alameh − *Department of Medicine, University of Pennsylvania, Philadelphia, Pennsylvania 19104, United States; Penn Institute for RNA Innovation, Perelman School of Medicine, Philadelphia, Pennsylvania 19104, United States*

Drew Weissman − *Department of Medicine, University of Pennsylvania, Philadelphia, Pennsylvania 19104, United States; Penn Institute for RNA Innovation, Perelman School of Medicine, Philadelphia, Pennsylvania 19104, United States;* orcid.org/0000-0002-1501-6510

Complete contact information is available at: https://pubs.acs.org/10.1021/jacs.6c00080

Notes

The authors declare the following competing financial interest(s): H.M.Y., M.S.P., and M.J.M. have filed a provisional patent application based on the work. The remaining authors declare no conflicts of interest.

ACKNOWLEDGMENTS

H.M.Y., A.G.H., K.L.S., A.S.T., H.C.G., A.A., C.F.-E., E.L.H., and A.M.M. acknowledge support from the US National Science Foundation Graduate Research Fellowship. O.Z.C. acknowledges support from the National Science Foundation under Cooperative Agreement DBI - 2400135. M.J.M. was supported by a Burroughs Wellcome Fund Career Award at the Scientific Interface (CASI), the Cystic Fibrosis Foundation (MITCHE24I0), an American Cancer Society Research Scholar Grant (RSG-22-122-01-ET), and an NSF CAREER Award (CBET-2145491).

ABBREVIATIONS

LNP, lipid nanoparticle; mRNA, messenger RNA; aroLNP, aromatic LNP

REFERENCES

(1) Thomas, S. J.; Moreira, E. D.; Kitchin, N.; Absalon, J.; Gurtman, A.; Lockhart, S.; Perez, J. L.; Marc, G. P.; Polack, F. P.; Zerbini, C.; Bailey, R.; Swanson, K. A.; Xu, X.; Roychoudhury, S.; Koury, K.; Bouguermouh, S.; Kalina, W. V.; Cooper, D.; Frenck, R. W.; Hammitt, L. L.; Türeci, Ö.; Nell, H.; Schaefer, A.; Ünal, S.; Yang, Q.; Liberator, P.; Tresnan, D. B.; Mather, S.; Dormitzer, P. R.; Şahin, U.; Gruber, W. C.; Jansen, K. U. Safety and Efficacy of the BNT162b2 mRNA Covid-19 Vaccine through 6 Months. *N. Engl. J. Med.* **2021**, *385* (19), 1761−1773.

(2) Baden, L. R.; Sahly, H. M. E.; Essink, B.; Kotloff, K.; Frey, S.; Novak, R.; Diemert, D.; Spector, S. A.; Rouphael, N.; Creech, C. B.; McGettigan, J.; Khetan, S.; Segall, N.; Solis, J.; Brosz, A.; Fierro, C.; Schwartz, H.; Neuzil, K.; Corey, L.; Gilbert, P.; Janes, H.; Follmann, D.; Marovich, M.; Mascola, J.; Polakowski, L.; Ledgerwood, J.; Graham, B.

S.; Bennett, H.; Pajon, R.; Knightly, C.; Leav, B.; Deng, W.; Zhou, H.; Han, S.; Ivarsson, M.; Miller, J.; Zaks, T. Efficacy and Safety of the mRNA-1273 SARS-CoV-2 Vaccine. *N. Engl. J. Med.* **2021**, *384* (5), 403−416.
(3) Zhao, Y.; Huang, L.Lipid Nanoparticles for Gene Delivery. In *Advances in Genetics*; Elsevier, 2014; Vol. *88*, pp 13−36 .
(4) Mardomi, A.; Mousavi, T.; Farnood, F.; Khosroshahi, H. T. Genotoxicity: A Neglected but Potentially Critical Aspect of Adenoviral COVID-19 Vaccines. *Future Virol.* **2023**, *18* (15), 971−973.
(5) Swetha, K.; Kotla, N. G.; Tunki, L.; Jayaraj, A.; Bhargava, S. K.; Hu, H.; Bonam, S. R.; Kurapati, R. Recent Advances in the Lipid Nanoparticle-Mediated Delivery of mRNA Vaccines. *Vaccines* **2023**, *11* (3), No. 658.
(6) Huang, X.; Ma, Y.; Ma, G.; Xia, Y. Unlocking the Therapeutic Applicability of LNP-mRNA: Chemistry, Formulation, and Clinical Strategies. *Research* **2024**, *7*, No. 0370.
(7) Cheng, Q.; Wei, T.; Farbiak, L.; Johnson, L. T.; Dilliard, S. A.; Siegwart, D. J. Selective Organ Targeting (SORT) Nanoparticles for Tissue-Specific mRNA Delivery and CRISPR−Cas Gene Editing. *Nat. Nanotechnol.* **2020**, *15* (4), 313−320.
(8) Simonsen, J. B. Lipid Nanoparticle-Based Strategies for Extrahepatic Delivery of Nucleic Acid Therapies − Challenges and Opportunities. *J. Controlled Release* **2024**, *370*, 763−772.
(9) Wang, J.; Ding, Y.; Chong, K.; Cui, M.; Cao, Z.; Tang, C.; Tian, Z.; Hu, Y.; Zhao, Y.; Jiang, S. Recent Advances in Lipid Nanoparticles and Their Safety Concerns for mRNA Delivery. *Vaccines* **2024**, *12* (10), No. 1148.
(10) Zaleski, M. H.; Chase, L. S.; Hood, E. D.; Wang, Z.; Nong, J.; Espy, C. L.; Zamora, M. E.; Wu, J.; Morrell, L. J.; Muzykantov, V. R.; Myerson, J. W.; Brenner, J. S. Conjugation Chemistry Markedly Impacts Toxicity and Biodistribution of Targeted Nanoparticles, Mediated by Complement Activation. *Adv. Mater.* **2025**, *37* (5), No. 2409945.
(11) Albertsen, C. H.; Kulkarni, J. A.; Witzigmann, D.; Lind, M.; Petersson, K.; Simonsen, J. B. The Role of Lipid Components in Lipid Nanoparticles for Vaccines and Gene Therapy. *Adv. Drug Delivery Rev.* **2022**, *188*, No. 114416.
(12) Han, X.; Zhang, H.; Butowska, K.; Swingle, K. L.; Alameh, M.-G.; Weissman, D.; Mitchell, M. J. An Ionizable Lipid Toolbox for RNA Delivery. *Nat. Commun.* **2021**, *12* (1), No. 7233.
(13) Padilla, M. S.; Mrksich, K.; Wang, Y.; Haley, R. M.; Li, J. J.; Han, E. L.; El-Mayta, R.; Kim, E. H.; Dias, S.; Gong, N.; Teerdhala, S. V.; Han, X.; Chowdhary, V.; Xue, L.; Siddiqui, Z.; Yamagata, H. M.; Kim, D.; Yoon, I.-C.; Wilson, J. M.; Radhakrishnan, R.; Mitchell, M. J. Branched Endosomal Disruptor (BEND) Lipids Mediate Delivery of mRNA and CRISPR-Cas9 Ribonucleoprotein Complex for Hepatic Gene Editing and T Cell Engineering. *Nat. Commun.* **2025**, *16* (1), No. 996.
(14) Han, X.; Xu, J.; Xu, Y.; Alameh, M.-G.; Xue, L.; Gong, N.; El-Mayta, R.; Palanki, R.; Warzecha, C. C.; Zhao, G.; Vaughan, A. E.; Wilson, J. M.; Weissman, D.; Mitchell, M. J. In Situ Combinatorial Synthesis of Degradable Branched Lipidoids for Systemic Delivery of mRNA Therapeutics and Gene Editors. *Nat. Commun.* **2024**, *15* (1), No. 1762.
(15) Fenton, O. S.; Kauffman, K. J.; McClellan, R. L.; Appel, E. A.; Dorkin, J. R.; Tibbitt, M. W.; Heartlein, M. W.; DeRosa, F.; Langer, R.; Anderson, D. G. Bioinspired Alkenyl Amino Alcohol Ionizable Lipid Materials for Highly Potent In Vivo mRNA Delivery. *Adv. Mater.* **2016**, *28* (15), 2939−2943.
(16) Cornebise, M.; Narayanan, E.; Xia, Y.; Acosta, E.; Ci, L.; Koch, H.; Milton, J.; Sabnis, S.; Salerno, T.; Benenato, K. E. Discovery of a Novel Amino Lipid That Improves Lipid Nanoparticle Performance through Specific Interactions with mRNA. *Adv. Funct. Mater.* **2022**, *32* (8), No. 2106727.
(17) Kanjilal, P.; Dutta, K.; Thayumanavan, S. Thiol-Disulfide Exchange as a Route for Endosomal Escape of Polymeric Nanoparticles. *Angew. Chem., Int. Ed.* **2022**, *61* (37), No. e202209227.
(18) Li, Y.; Cao, Y.; Bai, H.; Zhang, L.; Chen, B.; Wu, C.; Shuai, Q.; Yan, Y. Incorporation of Disulfide Bonds into Ionizable Lipids Enables Efficient Splenic mRNA Delivery and Potent Immunotherapy in Mice. *Chem. Eng. J.* **2025**, *516*, No. 164285.
(19) Liu, J.; Chang, J.; Jiang, Y.; Meng, X.; Sun, T.; Mao, L.; Xu, Q.; Wang, M. Fast and Efficient CRISPR/Cas9 Genome Editing In Vivo Enabled by Bioreducible Lipid and Messenger RNA Nanoparticles. *Adv. Mater.* **2019**, *31*, No. 1902575, DOI: 10.1002/adma.201902575.
(20) Ni, H.; Hatit, M. Z. C.; Zhao, K.; Loughrey, D.; Lokugamage, M. P.; Peck, H. E.; Cid, A. D.; Muralidharan, A.; Kim, Y.; Santangelo, P. J.; Dahlman, J. E. Piperazine-Derived Lipid Nanoparticles Deliver mRNA to Immune Cells in Vivo. *Nat. Commun.* **2022**, *13* (1), No. 4766.
(21) Love, K. T.; Mahon, K. P.; Levins, C. G.; Whitehead, K. A.; Querbes, W.; Dorkin, J. R.; Qin, J.; Cantley, W.; Qin, L. L.; Racie, T.; Frank-Kamenetsky, M.; Yip, K. N.; Alvarez, R.; Sah, D. W. Y.; de Fougerolles, A.; Fitzgerald, K.; Koteliansky, V.; Akinc, A.; Langer, R.; Anderson, D. G. Lipid-like Materials for Low-Dose, in Vivo Gene Silencing. *Proc. Natl. Acad. Sci. U.S.A.* **2010**, *107* (5), 1864−1869.
(22) Shepherd, S. J.; Warzecha, C. C.; Yadavali, S.; El-Mayta, R.; Alameh, M.-G.; Wang, L.; Weissman, D.; Wilson, J. M.; Issadore, D.; Mitchell, M. J. Scalable mRNA and siRNA Lipid Nanoparticle Production Using a Parallelized Microfluidic Device. *Nano Lett.* **2021**, *21* (13), 5671−5680.
(23) Sabnis, S.; Kumarasinghe, E. S.; Salerno, T.; Mihai, C.; Ketova, T.; Senn, J. J.; Lynn, A.; Bulychev, A.; McFadyen, I.; Chan, J.; Almarsson, Ö.; Stanton, M. G.; Benenato, K. E. A Novel Amino Lipid Series for mRNA Delivery: Improved Endosomal Escape and Sustained Pharmacology and Safety in Non-Human Primates. *Mol. Ther.* **2018**, *26* (6), 1509−1519.
(24) Zhang, T.; Yin, H.; Li, Y.; Yang, H.; Ge, K.; Zhang, J.; Yuan, Q.; Dai, X.; Naeem, A.; Weng, Y.; Huang, Y.; Liang, X.-J. Optimized Lipid Nanoparticles (LNPs) for Organ-Selective Nucleic Acids Delivery *in Vivo*. *iScience* **2024**, *27* (6), No. 109804.
(25) Strachan, J. B.; Dyett, B. P.; Nasa, Z.; Valery, C.; Conn, C. E. Toxicity and Cellular Uptake of Lipid Nanoparticles of Different Structure and Composition. *J. Colloid Interface Sci.* **2020**, *576*, 241−251.
(26) Ung, T.; Rutledge, N. S.; Weiss, A. M.; Esser-Kahn, A. P.; Deak, P. Cell-Targeted Vaccines: Implications for Adaptive Immunity. *Front. Immunol.* **2023**, *14*, No. 1221008.
(27) Abakushina, E. V.; Popova, L. I.; Zamyatnin, A. A.; Werner, J.; Mikhailovsky, N. V.; Bazhin, A. V. The Advantages and Challenges of Anticancer Dendritic Cell Vaccines and NK Cells in Adoptive Cell Immunotherapy. *Vaccines* **2021**, *9* (11), No. 1363.
(28) Roberts, E. W.; Broz, M. L.; Binnewies, M.; Headley, M. B.; Nelson, A. E.; Wolf, D. M.; Kaisho, T.; Bogunovic, D.; Bhardwaj, N.; Krummel, M. F. Critical Role for CD103+/CD141+ Dendritic Cells Bearing CCR7 for Tumor Antigen Trafficking and Priming of T Cell Immunity in Melanoma. *Cancer Cell* **2016**, *30* (2), 324−336.
(29) Ghosh, D.; Jiang, W.; Mukhopadhyay, D.; Mellins, E. D. New Insights into B Cells as Antigen Presenting Cells. *Curr. Opin. Immunol.* **2021**, *70*, 129−137.
(30) Hosseini-Kharat, M.; Bremmell, K. E.; Prestidge, C. A. Why Do Lipid Nanoparticles Target the Liver? Understanding of Biodistribution and Liver-Specific Tropism. *Mol. Ther.–Methods Clin. Dev.* **2025**, *33* (1), No. 101436.
(31) Wang, X.; Yuen, T. T.-T.; Dou, Y.; Hu, J.; Li, R.; Zeng, Z.; Lin, X.; Gong, H.; Chan, C. H.-C.; Yoon, C.; Shuai, H.; Ho, D. T.-Y.; Hung, I. F.-N.; Zhang, B.-Z.; Chu, H.; Huang, J.-D. Vaccine-Induced Protection against SARS-CoV-2 Requires IFN-γ-Driven Cellular Immune Response. *Nat. Commun.* **2023**, *14* (1), No. 3440.
(32) Normal Liver Histology 101 | AASLD. https://www.AASLD.org/liver-fellow-network/core-series/pathology-pearls/normal-liver-histology-101. (accessed December 02, 2025).
(33) Tanaka, H.; Sakurai, Y.; Anindita, J.; Akita, H. Development of Lipid-like Materials for RNA Delivery Based on Intracellular Environment-Responsive Membrane Destabilization and Spontaneous Collapse. *Adv. Drug Delivery Rev.* **2020**, *154*−*155*, 210−226.
(34) Kimura, S.; Okada, K.; Matsubara, N.; Lyu, F.; Tsutsumi, S.; Kimura, Y.; Hashiya, F.; Inagaki, M.; Abe, N.; Abe, H. In Vivo Demonstration of Enhanced mRNA Delivery by Cyclic Disulfide-

Containing Lipid Nanoparticles for Facilitating Endosomal Escape. *RSC Med. Chem.* **2025**, *16* (9), 4122−4137.
(35) Laurent, Q.; Martinent, R.; Lim, B.; Pham, A.-T.; Kato, T.; López-Andarias, J.; Sakai, N.; Matile, S. Thiol-Mediated Uptake. *JACS Au* **2021**, *1* (6), 710−728.
(36) van Duikeren, S.; Fransen, M. F.; Redeker, A.; Wieles, B.; Platenburg, G.; Krebber, W.-J.; Ossendorp, F.; Melief, C. J. M.; Arens, R. Vaccine-Induced Effector-Memory CD8+ T Cell Responses Predict Therapeutic Efficacy against Tumors. *J. Immunol.* **2012**, *189* (7), 3397−3403.
(37) Vasconcelos, J. R.; Dominguez, M. R.; Araújo, A. F.; Ersching, J.; Tararam, C. A.; Bruna-Romero, O.; Rodrigues, M. M. Relevance of Long-Lived CD8+ T Effector Memory Cells for Protective Immunity Elicited by Heterologous Prime-Boost Vaccination. *Front. Immunol.* **2012**, *3*, No. 358.
(38) Milner, J. J.; Nguyen, H.; Omilusik, K.; Reina-Campos, M.; Tsai, M.; Toma, C.; Delpoux, A.; Boland, B. S.; Hedrick, S. M.; Chang, J. T.; Goldrath, A. W. Delineation of a Molecularly Distinct Terminally Differentiated Memory CD8 T Cell Population. *Proc. Natl. Acad. Sci. U.S.A.* **2020**, *117* (41), 25667−25678.
(39) Hassett, K. J.; Rajlic, I. L.; Bahl, K.; White, R.; Cowens, K.; Jacquinet, E.; Burke, K. E. mRNA Vaccine Trafficking and Resulting Protein Expression after Intramuscular Administration. *Mol. Ther. Nucleic Acids* **2024**, *35* (1), No. 102083.
(40) Buckley, M.; Araínga, M.; Maiorino, L.; Pires, I. S.; Kim, B. J.; Michaels, K. K.; Dye, J.; Qureshi, K.; Zhang, Y. J.; Mak, H.; Steichen, J. M.; Schief, W. R.; Villinger, F.; Irvine, D. J. Visualizing Lipid Nanoparticle Trafficking for mRNA Vaccine Delivery in Non-Human Primates. *Mol. Ther.* **2025**, *33* (3), 1105−1117.
(41) Di, J.; Du, Z.; Wu, K.; Jin, S.; Wang, X.; Li, T.; Xu, Y. Biodistribution and Non-Linear Gene Expression of mRNA LNPs Affected by Delivery Route and Particle Size. *Pharm. Res.* **2022**, *39* (1), 105−114.
(42) Paunovska, K.; Da Silva Sanchez, A. J.; Lokugamage, M. P.; Loughrey, D.; Echeverri, E. S.; Cristian, A.; Hatit, M. Z. C.; Santangelo, P. J.; Zhao, K.; Dahlman, J. E. The Extent to Which Lipid Nanoparticles Require Apolipoprotein E and Low-Density Lipoprotein Receptor for Delivery Changes with Ionizable Lipid Structure. *Nano Lett.* **2022**, *22* (24), 10025−10033.
(43) Jang, D.-i.; Lee, A.-H.; Shin, H.-Y.; Song, H.-R.; Park, J.-H.; Kang, T.-B.; Lee, S.-R.; Yang, S.-H. The Role of Tumor Necrosis Factor Alpha (TNF-α) in Autoimmune Disease and Current TNF -α Inhibitors in Therapeutics. *Int. J. Mol. Sci.* **2021**, *22* (5), No. 2719.
(44) Trevejo, J. M.; Marino, M. W.; Philpott, N.; Josien, R.; Richards, E. C.; Elkon, K. B.; Falck-Pedersen, E. TNF-α-Dependent Maturation of Local Dendritic Cells Is Critical for Activating the Adaptive Immune Response to Virus Infection. *Proc. Natl. Acad. Sci. U.S.A.* **2001**, *98* (21), 12162−12167.
(45) Zawawi, Z. M.; Kalyanasundram, J.; Zain, R. M.; Thayan, R.; Basri, D. F.; Yap, W. B. Prospective Roles of Tumor Necrosis Factor-Alpha (TNF-α) in COVID-19: Prognosis, Therapeutic and Management. *Int. J. Mol. Sci.* **2023**, *24* (7), No. 6142.
(46) Avau, A.; Matthys, P. Therapeutic Potential of Interferon-γ and Its Antagonists in Autoinflammation: Lessons from Murine Models of Systemic Juvenile Idiopathic Arthritis and Macrophage Activation Syndrome. *Pharmaceuticals* **2015**, *8* (4), 793−815.
(47) Cao, X.; Manhas, A.; Chen, Y.-I.; Caudal, A.; Mondejar-Parreño, G.; Zhu, W.; Liu, W.; Kong, X.; Zeng, W.; Liu, L.; Zhao, S. R.; Jahng, J. W. S.; Utz, P. J.; Nadeau, K. C.; Nishiga, M.; Wu, J. C. Inhibition of CXCL10 and IFN-γ Ameliorates Myocarditis in Preclinical Models of SARS-CoV-2 mRNA Vaccination. *Sci. Transl. Med.* **2025**, *17* (828), No. eadq0143.
(48) Hailemichael, Y.; Johnson, D. H.; Abdel-Wahab, N.; Foo, W. C.; Bentebibel, S.-E.; Daher, M.; Haymaker, C.; Wani, K.; Saberian, C.; Ogata, D.; Kim, S. T.; Nurieva, R.; Lazar, A. J.; Abu-Sbeih, H.; Fa-ak, F.; Matthew, A.; Wang, Y.; Falohun, A.; Trinh, V.; Zobniw, C.; Spillson, C.; Burks, J. K.; Awiwi, M.; Elsayes, K.; Soto, L. S.; Melendez, B. D.; Davies, M.; Wargo, J.; Curry, J.; Yee, C.; Lizee, G. A.; Singh, S.; Sharma, P.; Allison, J. P.; Hwu, P.; Ekmekcioglu, S.; Diab, A. Interleukin-6 Blockade Abrogates Immunotherapy Toxicity and Promotes Tumor Immunity. *Cancer Cell* **2022**, *40* (5), 509−523.e6.
(49) Sterling, J. K.; Kam, T.-I.; Guttha, S.; Park, H.; Baumann, B.; Mehrabani-Tabari, A. A.; Schultz, H.; Anderson, B.; Alnemri, A.; Chou, S.-C.; Troncoso, J. C.; Dawson, V. L.; Dawson, T. M.; Dunaief, J. L. Interleukin-6 Triggers Toxic Neuronal Iron Sequestration in Response to Pathological α-Synuclein. *Cell Rep.* **2022**, *38* (7), No. 110358.
(50) Yang, Y.; Zhang, Y.; Xing, X.; Xu, G.; Lin, X.; Wang, Y.; Chen, M.; Wang, C.; Zhang, B.; Han, W.; Hu, X. IL-6 Translation Is a Therapeutic Target of Human Cytokine Release Syndrome. *J. Exp. Med.* **2023**, *220* (11), No. e20230577.
(51) Liu, A.; Wang, X. The Pivotal Role of Chemical Modifications in mRNA Therapeutics. *Front. Cell Dev. Biol.* **2022**, *10*, No. 901510.
(52) Xu, Y.; Gong, F.; Golubovic, A.; Strilchuk, A.; Chen, J.; Zhou, M.; Dong, S.; Seto, B.; Li, B. Rational Design and Modular Synthesis of Biodegradable Ionizable Lipids via the Passerini Reaction for mRNA Delivery. *Proc. Natl. Acad. Sci. U.S.A.* **2025**, *122* (5), No. e2409572122.
(53) Wang, W.; Chen, K.; Jiang, T.; Wu, Y.; Wu, Z.; Ying, H.; Yu, H.; Lu, J.; Lin, J.; Ouyang, D. Artificial Intelligence-Driven Rational Design of Ionizable Lipids for mRNA Delivery. *Nat. Commun.* **2024**, *15* (1), No. 10804.
(54) Zhang, W.; Pfeifle, A.; Lansdell, C.; Frahm, G.; Cecillon, J.; Tamming, L.; Gravel, C.; Gao, J.; Raman, S. N. T.; Wang, L.; Sauve, S.; Rosu-Myles, M.; Li, X.; Johnston, M. J. W. The Expression Kinetics and Immunogenicity of Lipid Nanoparticles Delivering Plasmid DNA and mRNA in Mice. *Vaccines* **2023**, *11* (10), No. 1580.
(55) Hassett, K. J.; Benenato, K. E.; Jacquinet, E.; Lee, A.; Woods, A.; Yuzhakov, O.; Himansu, S.; Deterling, J.; Geilich, B. M.; Ketova, T.; Mihai, C.; Lynn, A.; McFadyen, I.; Moore, M. J.; Senn, J. J.; Stanton, M. G.; Almarsson, Ö.; Ciaramella, G.; Brito, L. A. Optimization of Lipid Nanoparticles for Intramuscular Administration of mRNA Vaccines. *Mol. Ther.–Nucleic Acids* **2019**, *15*, 1−11.